Heliyon

ELSEVIER

Received:
24 November 2015
Revised:
20 March 2016
Accepted:
26 April 2016

Heliyon 2 (2016) e00107

Absorbable energy monitoring scheme: new design protocol to test vehicle structural crashworthiness

Sunday M. Ofochebe [a,*], **Samuel O. Enibe** [b], **Chigbogu G. Ozoegwu** [a]

[a] *Department of Mechanical Engineering, Nnamdi Azikiwe University Awka, Nigeria*

[b] *Department of Mechanical Engineering, University of Nigeria, Nsukka, Nigeria*

* Corresponding author.

E-mail address: aa_zee2@yahoo.com (S.M. Ofochebe).

Abstract

In vehicle crashworthiness design optimization detailed system evaluation capable of producing reliable results are basically achieved through high-order numerical computational (HNC) models such as the dynamic finite element model, mesh-free model etc. However the application of these models especially during optimization studies is basically challenged by their inherent high demand on computational resources, conditional stability of the solution process, and lack of knowledge of viable parameter range for detailed optimization studies. The absorbable energy monitoring scheme (AEMS) presented in this paper suggests a new design protocol that attempts to overcome such problems in evaluation of vehicle structure for crashworthiness. The implementation of the AEMS involves studying crash performance of vehicle components at various absorbable energy ratios based on a 2DOF lumped-mass-spring (LMS) vehicle impact model. This allows for prompt prediction of useful parameter values in a given design problem. The application of the classical one-dimensional LMS model in vehicle crash analysis is further improved in the present work by developing a critical load matching criterion which allows for quantitative interpretation of the results of the abstract model in a typical vehicle crash design. The adequacy of the proposed AEMS for preliminary vehicle crashworthiness design is demonstrated in this paper, however its extension

http://dx.doi.org/10.1016/j.heliyon.2016.e00107

to full-scale design-optimization problem involving full vehicle model that shows greater structural detail requires more theoretical development.

Keyword: Engineering

1. Introduction

The fatality resulting from vehicle crash in road accidents has been identified as the most regrettable influence of ground vehicle transportation on human being. While the incidence of road accident remains ever unpredictable, a lot of preventive rules and severity control means have been developed. The need to attain a comfort level in crash injury protection continues to drive researchers to the study of vehicle crashworthiness. Although, quite commendable improvements in vehicle crash safety have been recorded over the years through the available crash injury protection technologies and crash avoidance schemes, yet the complexity of vehicle crash problem remains a challenge to accurate crashworthiness design. The major issue which motivates the present study is the persistent difficulty in achieving what could be considered the most desirable crash performance within a typical design space with the available optimization techniques. The conventional design-optimization methods seem to rely on the accuracy of high-order numerical computational (HNC) models for attaining valid assessment of vehicle crashworthiness. Literal evidence to this claim is found in the reviewed articles [1, 2, 3]. Although HNC methods are quite robust in achieving reliable results and valid conclusions, yet their implementation to the details of vehicle structural complexities, places a considerably high demands on computation resources. With the dynamics of vehicle impact being highly nonlinear, the existence of local optima in the parameter space is highly anticipated. The attainment of the most desirable system performance in a global optimization study via such high demanding computation methods is usually uncertain. Since the investigations must be conducted within a sufficiently close data range over the entire design space, completing the optimization steps progressively becomes prohibitively expensive as the size of sampling space increases. As a way forward, designers and structural analysts tend to employ previous experience/knowledge of the system behavior for selecting a useful parameter range for detailed design investigation and optimization study. The result of this trend is the continual marginal improvements and the fluctuations in general crash performance identified in the existing vehicle models [4].

In the design of entirely new vehicle structure with completely unknown crash behavior, designer's experience may not guarantee the desired success in a stretch of optimization study since there is greater tendency of choosing an invalid parameter range at which the stability of the computation process may be adversely affected. This implies further frustration of the design- optimization process. In

http://dx.doi.org/10.1016/j.heliyon.2016.e00107

search of more efficient computation approach needed to facilitate the design of new vehicle structure, it is conceived in the present study that instead of relying on designer's experience or known system behavior for making preliminary considerations required to ensure improved performance of the system or to define a valid parameter range for detailed optimization study, a 'knowledge-base-integrated' design procedure could be developed. In other words, the design-optimization protocol could be made to include some form of pre-investigation of the design problem over a wide parameter range preferably using abstract model(s) prior to full-scale optimization study. The preliminary study is intended to build a knowledge-base of the anticipated overall system behavior using certain computationally efficient method. In the process, a steep ascent to a viable parameter range which holds a good prospect of revealing the most desirable crash response is verified following a formal procedure. The 2DOF lumped mass spring (LMS) system which is capable of predicting the crash behavior of the vehicle impact system based on the known static crush behaviors of the structural components is considered an appropriate resource for pursuing this important design objective. However, the crucial demands for a reliable accuracy and a more detailed representation of the system coupled with the additional task involved in translating the results of the one-dimensional LMS model to real design quantities such as column dimensions and mechanical properties required during actual component formulation generally oppose wide application of LMS models in the field of vehicle crashworthiness studies [5, 6, 7, 8, 9, 10]. Nevertheless, the present study noted that the application of such an abstract model could be extended a little further to preliminary evaluation of crash performance of vehicle structure in a typical design problem. The necessary tasks involve formulating the model in a nonlinear framework capable of predicting the dynamic behaviors of the impact system to a certain reasonable details with an acceptable level of accuracy. The other highlighted issue of interpreting the results of the model in a real design problem is resolved in this study by introducing a universal design criterion in terms of the critical load of the structural members which applies overtly to both the LMS model and the equivalent simplified FE model; both of which were considered suitable for pursing the preliminary design objectives. This led to a new theoretical concept known as the *critical load matching criteria.* The theory of critical load matching developed in this study follows from the knowledge that the distribution of impact load (i.e. the fractions of the total impact energy of the system absorbed during deformation of specific structural component) is automatically controlled by the relative load strengths of the components [11]. It then implies that either the absorbable energy or the critical load of the components could be chosen alternatively as the design variable depending on the applicable computation model for monitoring the system performance. This design principle preferably called the *absorbable energy monitoring scheme* (AEMS) reduces the tasks involved in formulating the components for proper energy absorption, and

http://dx.doi.org/10.1016/j.heliyon.2016.e00107

defining a viable parameter range for detailed study to judicious selection of the load capacities of the components such that certain desirable energy absorption pattern (of known crash performances) is guaranteed. With the proposed absorbable energy monitoring system fully implemented on LMS model, the translation of the resulting inertial and stiffness properties of the system into regular design quantities (mechanical properties and geometry of the design components) becomes a lot more straightforward.

Since achieving the needed comfort in crash injury protection especially as it relates to structural intrusion into the passenger compartment, and occupants' acceleration in the midst of deforming vehicle structure remains a challenge to designers, the virtue of both passive and active crash severity control systems and cushioning facilities such as; collapsible steering column/control levers, flexible sit-belt, air-bag and other subsidiary restraint systems are consistently being emphasized [12, 13, 14, 15]. By and large, deformation of vehicle structure remains the known active practical means to ensure adequate absorption of impact energy which essentially combines with the cushioning effects of safety gadgets to grant the desired vehicle occupants protection from injury in survivable crashes. It is noted that further improvements on the state-of-art vehicle crash injury protection technologies could be achieved through better evaluation of the system during product design. The proposed AEMS is a structural design concept which ultimately aims to quantify the energy absorption capacities of vehicle structural components using their known geometric/mechanical properties such that if a desirable energy absorption pattern is substantially defined for the system on theoretical basis, the selection of workable values of actual design variables during component formulation and parameter optimization becomes much more precise. This idea is fully explored in this paper using a case study of an idealized front-half vehicle model displaying a head-on collision against a rigid barrier.

2. Methodology

The 2DOF lumped mass spring (LMS) model proposed for vehicle crash simulation in a preliminary design process is a simple computational model in which the vehicle crash scenario is idealized using a system of three rigid masses connected to each other via two nonlinear springs. The masses represent the undeformable inertial components which include; an infinite static mass used to model the barrier and two dynamic masses used to model the payload (body) mass m_1 and the engine mass m_2. On the other hand, the nonlinear springs represent the deformable vehicle structural components. The model is formulated to capture the non-linear dynamics of the crash phenomenon (including the gross motion of compliant/rigid components and the energy absorption sequence) in a rather simplistic sense. In line with the basic principles of crashworthiness design and LMS system modeling procedure, the formulation the 2DOF vehicle impact model

http://dx.doi.org/10.1016/j.heliyon.2016.e00107

presented in Fig. 1, utilized the following assumptions considered for a conventional integral body structure with transversely laid out engine;

i. Collision type is full-lap frontal impact against a rigid barrier.

ii. The passenger compartment is lumped as the payload mass m_1, assuming it is sufficiently rigid to shield the occupants. The engine, suspension and the transmission system or drive train (which include the gearbox, clutch system and drive shaft) known to be structurally stronger than other front components are also considered un-deformable and collectively lumped as engine mass m_2.

iii. The total resistance of the structures forward and rearward to the engine mass separated by the engine mount depends on the dynamic stiffnesses of the non-linear springs and the spring deformation rate $\dot{\delta}$.

iv. The contributions to the dynamic resistance due to highly flexible or fragile non-structural members like cables, glasses, conduits etc. are considered negligible.

2.1. Equation of motion

Considering the equilibrium of the force system, the equation of motion of the impact system is written as (1).

$$m_1\ddot{x}_1 + F_1 = 0$$

$$m_2\ddot{x}_2 + F_2 - F_1 = 0 \tag{1}$$

Rewriting (1) in compact form;

$$M\ddot{X} + \overline{F} = 0 \tag{2}$$

M represents the mass matrix, $\ddot{X}$ the acceleration vector and $\overline{F}$ stands for the vector of the net nonlinear resistant forces generated in the system.

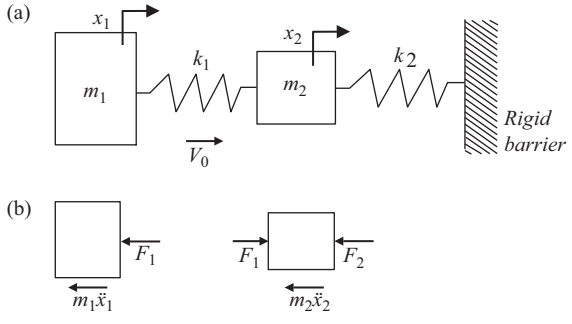

Fig. 1. (a) Two mass- spring system (b) equivalent force system.

http://dx.doi.org/10.1016/j.heliyon.2016.e00107

2.2. Force deformation analysis

The resistant forces F_j, (j = 1, 2) generated in the springs assume various forms during the impact motion. In order to incorporate the dynamics of F_j in the equilibrium of the system, the force-displacement characteristics of the components were reviewed. The load-deformation characteristics presented in Fig. 2a which leads to the identification of four distinct load zones $(zone\,1-4)$ is typical of a nonlinear spring subjected to a dynamic impact load [7, 8, 16]. Considering the gross motion of the components during impact, an approximate force-displacement diagram (Fig. 2b) is drawn to account for possible instances of structural displacement without effective resistance in the system. The nonlinear resistant force F_j of the springs is characterized completely in the dynamic states via the load zoning formula (3). Eq. (3) accounts for the various forms identified by F_j from the initial state of the motion when a component is possibly sensing the impact without providing any significant resistance $(zone\,Z0)$ through cases of stiff elastic motion (loading, unloading or reloading) against rigid wall $(zone\,Z1)$ and subsequent plastic flow (or localized buckling) under settling force $(zones\,Z2\,and\,Z3)$, up to the final case when the component becomes fully compressed, and transforms to solid mass. The transition from *zone* 3 to *zone* 4 of the deformation-load path (referred to as structural decomposition) by any component in the dynamic states is uncertain. The reason being that at this stage the residual impact load is readily transmitted to the next compliant structure while the fully compressed component returns to *zone* $Z0$. The contribution of *zone* 4 to the dynamic energy absorption scheme is thus considered negligible.

$$F_j = \begin{cases} k_{p,j}\delta_j; for\ displacement\ in\ zone\ Z1 \\ F_{s,j}(\nu + \xi\delta)_j; for\ displacement\ in\ zone\ Z2 \\ F_{s,j}; for\ displacement\ in\ zone\ Z3 \\ 0; for\ displacement\ in\ zone\ Z0 \end{cases} \tag{3a}$$

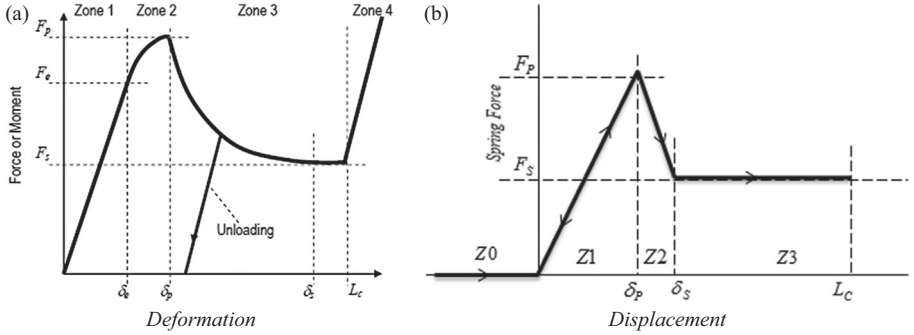

Fig. 2. (a) Typical load-deformation behavior of nonlinear springs and (b) approximate force displacement diagram representing gross motion of a structural component under dynamic impact load.

http://dx.doi.org/10.1016/j.heliyon.2016.e00107

$$\nu = \frac{qs - p}{q - p}; \xi = \frac{1 - s}{L_c(q - p)} \tag{3b}$$

Where δ_j stands for instantaneous deformation of a given spring j; $k_{p,j}$ and $F_{s,j}$ represent the peak (elastic) stiffness and the mean (plastic) resistance of the spring respectively. The parameters named L_c,$p\left(= \delta_p/L_c\right)$, $q(= \delta_s/L_c)$ and $s\left(= F_p/F_s\right)$ are the crush characteristics of the nonlinear spring which are clearly described in Fig. 2.

Displacements found in zones Z1, Z2 and Z3 indicated in the displacement-load path (Fig. 2b) correspond to structural deformation and contribute substantially to energy absorption scheme. Such zones are regarded in this paper as active load zone, while zone Z0 and zone 4 of the deformation-load path which lead to total transmission of impact load and insignificant energy absorption respectively are classified as idle load zone. The transition from idle zone through the active zone (s) back to idle zone during the impact leads to a corresponding change in the equilibrium of the system. These changes must be observed to arrive at the detailed governing equation(s) of motion.

The total contribution to the net resistant force due to plastic deformation of a specific spring is given as the sum of the partial resistances recorded in the three active load zones

$$F_j = F_{j,1} + F_{j,2} + F_{j,3} \tag{4}$$

The evaluation of the system response via the proposed method requires that the spring tuning parameters $F_{p,j}$, $F_{s,j}$ and $\overline{\mathrm{k}}_j$ which describe the load path of structural resistance must be quantified in the dynamic state. This implies that the amount of impact load received by every individual component which determines the contribution of the component to the dynamic energy absorption sequence (E_j) is known (preferably for the 2DOF system) in terms of the relative energy absorption capacity $(r = E_2/E_1)$ of the components. The proposed AEMS attempts to evaluate the system performance at various values of r such that any system configuration(s) leading to a desired performance are revealed. The success of this approach lies on proper characterization of E_j upon which the tuning parameters are estimated. In view of the complications and the usual rise in computation time associated with tracing the details of the actual load path in the overall solution of E_j, the linearized form illustrated by the approximate force displacement diagram of Fig. 2b is considered in developing the solution algorithm; assuming that a sufficient estimate of the force-deformation behavior and the energy absorption sequence could be achieved in the active load zones (Z1, Z2 and Z3) via the approximate displacement model. This consideration enables detailed programing of the structural deformation sequence with minimized cases of iterative switches in the solution steps that essentially grants computational efficiency.

http://dx.doi.org/10.1016/j.heliyon.2016.e00107

Considering the energy conservation principle;

$$E = \Sigma E_j = 0.5\gamma m V_0^2 \tag{5}$$

and material balance

$$m = \Sigma m_i \tag{6}$$

The total absorbable energy of the system E is quantified by the initial kinetic energy of the vehicle, while the energy absorption capacity of an individual nonlinear spring E_j is quantified by the stiffness/damping properties of the structural components. V_0 is the initial impact velocity and γ is the tolerance factor (or system adjustment variable).

Since every displacement measured in the active load zone corresponds to structural deformation, the individual energy absorption capacity E_j of the springs is quantified by the area enclosed by the force-displacement curve presented in Fig. 2b i.e.

$$E_j = 0.5\delta_{s,j}F_{p,j} + F_{s,j}\left[\left(L_c - 0.5\left(\delta_{s,j} + \delta_{p,j}\right)\right)\right] \tag{7}$$

Introducing the absorbable energy ratio $(r = E_2/E_1)$ as design variable for the 2DOF system, then from (5)

$$E_1 = 0.5\gamma m {V_0}^2 (1+r)^{-1} \tag{8a}$$

$$E_2 = rE_1 = 0.5\gamma m r {V_0}^2 (1+r)^{-1} \tag{8b}$$

Assuming the average dynamic behavior of the nonlinear springs reflects the known crush behaviors (i.e. $s_j = F_{p,j}/F_{s,j}$; $p_j = \delta_{p,j}/L_{c,j}$ *and* $q_j = \delta_{s,j}/L_{c,j}$), then the unknown spring tuning parameters including the dynamic peak force $\overline{F}_{p,j}$, the mean (steady) force $\overline{F}_{s,j}$ and the dynamic stiffness $\overline{k}_j$ under distributed impact load are written in terms of the known system variables as follows

$$\overline{F}_{s,j} = \frac{2E_j}{L_{c,j}\left[q_j\left(s_j - 1\right) - p_j + 2\right]} \tag{9}$$

Since $\overline{F}_{p,j} = s_j\overline{F}_{s,j}$, the mean dynamic stiffness $\overline{k}_j$ of a specific spring is then written as

$$\overline{k}_j = \frac{\overline{F}_{p,j}}{\overline{\delta}_{p,j}} = \frac{2s_jE_j}{p_jL_{c,j}^2[q_j(s_j-1) - p_j + 2]}; i = j = 1,2 \tag{10}$$

It is noted that while a deforming component may traverse all or some the stated load zones depending on the nature of the impact and structural configuration, the possibility of the different components appearing in different load zones at certain instance of the motion also exists. With the tuning parameters $\overline{F}_{s,j}$ and $\overline{k}_j$ already quantified by (9) and (10) respectively, the dynamic equilibrium of the system can

http://dx.doi.org/10.1016/j.heliyon.2016.e00107

now be explored for every observation of the spring system in the load zoning system. The thirteen possible cases of structural loading identified with the system is given in Table 1.

The notations $\vec{F}_{j,1}$, $\vec{F}_{j,2}$, $\vec{F}_{j,3}$, $\vec{F}_{j,0}$ and $F_{j,0'}$ were used to denote respective observations of a specific nonlinear spring j in; the linear elastic force zone, partial unloading zone, steady plastic force zone, fully compressed state and totally consumed state in the load path of deformation.

2.3. Solution algorithm

The motion of the impact system is governed by thirteen state differential equations obtained by writing the equilibrium of the force system for the observable cases of structural loading given in Table 1.

In any case, the dynamic equilibrium of the system is recalled from (2) considering the observable load zone(s) as;

$$M\ddot{X} + \Sigma_z \overline{F_z} = 0 \tag{11}$$

The subscript $z(= 1, 2, 3)$ is used to indicate the load zones associated with every contribution to the dynamic resistance. Eq. (11) could be expanded in form

$$M\ddot{X} + \alpha(F_p) + \beta(\delta, \dot{\delta}, F_s) + \psi(F_s, \dot{\delta}) = 0 \tag{12}$$

Where α, β and ψ are the nonlinear maps of the structural resistance in zone Z1, zone Z2 and zone Z3 respectively.

The solution program employs the general state-space transformation rule for $n \times m$ mass-spring systems [14].

$$x_i = \phi_{(2i-1),}$$

$$\dot{\phi}_k = \phi_{(k+1)} \text{ for: k=1,3,..2n}-1$$

$$\dot{\phi}_l = \ddot{\phi}_{(l-1)} \text{ for: l=2,4..2n} \tag{13}$$

This leads to the generalized state differential equation of motion for a particular case of structural loading (14).

Table 1. Observations of the nonlinear springs k_1 and k_2 in the load zoning system.

Observable cases of structural loading								
	$\vec{F}_{1,1}\vec{F}_{2,1}$	$\vec{F}_{1,1}\vec{F}_{2,2}$	$\vec{F}_{1,1}\vec{F}_{2,3}$	$\vec{F}_{1,1}\vec{F}_{2,0}$	$\vec{F}_{1,2}\vec{F}_{2,0}$	$\vec{F}_{1,3}\vec{F}_{2,0'}$	$\vec{F}_{2,1}\vec{F}_{1,2}$	$\vec{F}_{2,1}\vec{F}_{1,3}$
	$\vec{F}_{2,1}\vec{F}_{1,0}$	$\vec{F}_{2,2}\vec{F}_{1,0}$	$\vec{F}_{2,3}\vec{F}_{1,0'}$	$\vec{F}_{1,2}\vec{F}_{2,2}$	$\vec{F}_{1,3}\vec{F}_{2,3}$			

http://dx.doi.org/10.1016/j.heliyon.2016.e00107

$$m_{ij}\dot{\phi}_i + k_{ij}\phi_i + sign\dot{\delta}f_2 + sign\dot{\delta}f_3 = 0 \quad (14)$$

Where m_{ij} and k_{ij} represent the mass matrix (corresponding to the inertia force) and stiffness matrix (corresponding to the resistance in zone Z1) respectively. f_2 and f_3 represent the vectors of the dynamic forces found in zones Z2 and Z3 respectively, while ϕ_i and $\dot{\phi}_i$ denote the states of the masses during the impact motion. The detailed programing of the impact motion involves writing thirteen different sets of equation based on (14) for the thirteen possible cases of structural loading identified (one for each case) using the load zoning formula (3).

To complete the solution in line with the first objective of this study the distinct energy absorption capacities of the springs were first evaluated from eq. (8a) and (8b) for a specific value of r, which enable the calculation of $\overline{F}_{s,j}$, and $\overline{k}_j$ from (9) and (10) respectively. The crush characteristics p_j, q_j, s_j, $d_{s,j}$ and $L_{C,j}$ were considered for a typical compliant thin-walled elastoplastic column whose properties are given in Table 2. The resulting data were then applied for evaluating the system response through a computer program written to solve the governing equations, given the initial conditions $(\dot{x}_1 = \dot{x}_2 = V_0, x_1 = x_2 = 0)$. The development of the program employs simple logics that check the deformation state of the springs and select appropriate governing differential equation from the thirteen sets such that the displacements and velocities of the springs arising from the preceding state are automatically fed as initial conditions to the new governing equation of the present state. The solution was completed through numerical integration using ODE 45 solver found in MATLAB. The solver uses high-order Rung-kutta method. No critical time step is required for numerical stability. However, using the default error tolerance may lead to very low computation speed. Fast computation is normally achieved by choosing appropriate combination of real and absolute error tolerance setting in the odeset such as; 'odeset ('RelTol',1e-3,'AbsTol',1e-3)'.

2.4. Formalization of the proposed absorbable energy monitoring scheme for vehicle crashworthiness design

In crucial effort to formalize the proposed absorbable energy monitoring system for vehicle structural crashworthiness design, the present study endeavors to construct

Table 2. Parameters of LMS vehicle impact simulation model applied in the preliminary study.

Symbol	V_0	m_1	ρ	$L_{c,1}$	$L_{c,2}$	p_1	p_2	q_1	q_2	s_1	s_2	r
Value	10	820	0.25	0.25	0.25	0.01	0.02	0.015	0.025	3	3	variable
Unit	m/s	kg		m	m							

http://dx.doi.org/10.1016/j.heliyon.2016.e00107

a systematic procedure for applying the knowledge of the anticipated crash behavior of the system obtained through LMS simulation method to enhance selection of valid parameter range for detailed investigation of the impact system using the conventional finite element method (FEM). The task requires that a virtual model of the vehicle crash scenario is first constructed based on real vehicle structural geometry, using material/mechanical properties of a typical vehicle front structure. An equivalent LMS model is then formulated and used to give initial evaluation of the system, after which necessary adjustments to the FE model are directed towards translating certain desirable inertial and stiffness/damping properties predicted by the LMS approach to real sectional geometries and mechanical properties required in the FE formulation. The results obtained using both methods can then be compared at similar configuration of the system. The expectation is to see the extent to which the results of the highly abstract LMS modeling approach correspond to a more realistic prediction of the vehicle crash behavior.

In this study, the FE model for vehicle crash simulation is formulated as a virtual front-half vehicle model in which the remaining half of the vehicle is modeled as a rigid mass called the body mass. The suspension, engine and the transmission system are also assumed sufficiently rigid under normal impact condition and are collectively modeled as meshed solid box called the engine mass. The structural components are modeled as continues mesh of non-uniform shell elements capable of undergoing elastic-plastic deformation under impact condition. The body and the engine masses are connected to the vehicle structure via rigid beams. The material models for the energy absorbing components are considered general elasto-plastic. The mass values and boundary conditions are then specified based on typical service and test conditions respectively as shown in Table 3. Although the construction of the FE model presented in Fig. 3b also involves yet another level of abstraction (ignoring the details of other smaller components and non-structural members found in real vehicle system such as the radiator, cables, fenders etc.) yet it grants better physical representation of vehicle structure compared to the LMS model. The simplified FE model which essentially configures the impact system for easy manipulation of design variables in the context of the absorbable energy monitoring scheme is known to grant adequate

Table 3. Initial conditions of the masses applied in the FE model.

Vehicle mass/initial cond.	Body mass	Engine mass	Structural mass
Value (kg)	500	250	275
Initial displacement x_0 (m)	0	0	0
Initial Velocity $\dot{x}_0$ (m/s)	10	10	10

http://dx.doi.org/10.1016/j.heliyon.2016.e00107

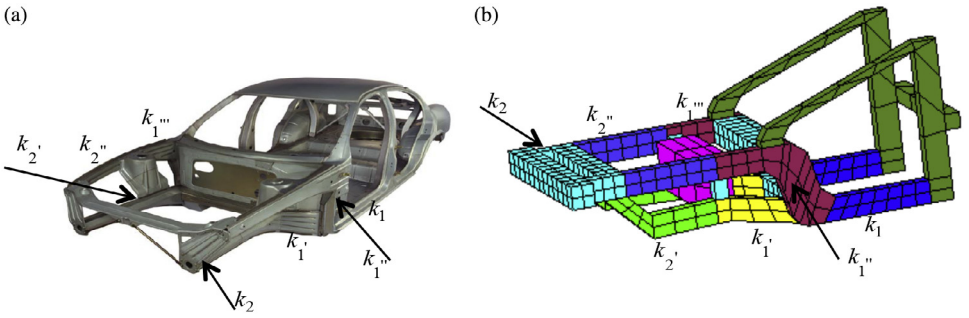

Fig. 3. (a) Real vehicle structure (b) the front-half FE model.

prediction of crash behavior of the full vehicle model in frontal impacts [17], and is thus considered suitable for making prompt decision for structural crashworthiness during prototype development.

It is known that plastic deformation initiates from the weakest structural zone irrespective of its location in the system. In typical mechanical modeling of vehicle front structure more than two structural regions of different geometries and material make-up are critically designed to comply with basic structural requirements such as; load bearing capacity, damping of high frequency vibration, aerodynamic stability, esthetics, etc. in addition to structural crashworthiness. The construction of the FE model is equally generally dependent on similar considerations. Excessive distortion, bending and other forms of catastrophic failures which could lead to excessive stretching/compression or complete separation of the element mesh must be controlled to avoid computation instabilities or total failure of the FE iteration process. Finite element modeling procedure allows for proper identification of structural regions. The number of observable crash mode is also expected to increase with number of distinct structural regions formed. However, desirable crash mode (*CM*) of the system is basically achieved in two unique stages of structural deformation featuring; early crushing of the foremost structures between the engine and the barrier in the first stage accompanied by certain rebound of the engine mass and later minimal deformation of the interior structures against the engine mass in the second stage. Thus further considerations necessary to restrict the crash sequence of the structures to what could be desirable in the FE approach is described using an equivalent spring system shown in Fig. 4.

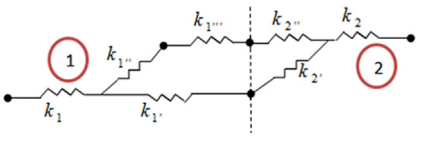

Fig. 4. Equivalent spring model of the main energy absorbing components.

http://dx.doi.org/10.1016/j.heliyon.2016.e00107

Fig. 4 depicts a spring system used to visualize the front-half vehicle structure in a comparable form with the 2DOF LMS model. A total of seven major energy absorbing members with designated stiffness $k_1, k_{1'} k_{1''}, k_{1'''}, k_{2'}, k_{2''}$ and k_2 were clearly identified in the system and grouped accordingly. The corresponding non-linear resistances of the entire structural system are represented in two dimensional space divided into two distinct regions '1′ and '2′ by an imaginary line that coincides with the axis of the engine mount. Each member of the FE model is assumed to be a virtual hollow rectangular column whose energy absorption potential depends on both the geometry and the mechanical properties. Since the integrity of the passenger compartment must be preserved while impact energy is transmitted towards the interior structures, it then implies that the cab structures k_1 and $k_{1''}$ must be sufficiently rigid. In other words;

$$k_1 \gg k_{1'} + k_{1''} \text{ and } k_{1''} \gg k_{1'''} \quad (15)$$

Also to ensure maximum transmission of impact energy into the interior structures the bumper beam and the other cross-members must be strong enough to withstand transverse loading which is capable of causing catastrophic failure. Such non-compliant members do not contribute significantly to energy absorption. Hence the upper columns $k_{1'''}, k_{2''}$ and the lower rails $k_{1'}, k_{2'}$ were selected as the sampling space. The Necessary considerations to material thickness, component geometry and boundary conditions were realized in the element mesh during the pre-processing of the FE model. The component design involves evaluation of the critical load P_{cr} and the maximum crushable length L_c of the various structural regions which must be completed before system iteration.

2.5. Determination of critical load of structural regions

Considering the geometry, material properties and load conditions of the main energy absorbing components shown in Fig. 3, an individual member can be visualized as intermediated column under distributed compressive load. Compressive loads/stresses in columns generally leads to two major types of elastic instabilities: global and local instabilities. Global instability becomes significant at sufficiently high value of slenderness ratio (S.R) and leads to *catastrophic failure* (global buckling) which is undesirable and must be minimized in the context of crashworthiness design. Local instability on the other hand causes desirable *permanent deformation* (localized buckling or function failure) more identified with columns of low S.R (l/ε) values. By and large, front vehicle structures are prone to these two failure modes at varying degrees. Thus, the derivation of the critical load and failure condition of the components is based on the *parabolic* equation for intermediate – length columns (16), which essentially accounts for the effects of component length [18].

http://dx.doi.org/10.1016/j.heliyon.2016.e00107

$$P_{cr}/A = S_y - \left(\frac{S_y}{2\pi}\frac{l}{\varepsilon}\right)^2 \frac{1}{CE_m};\ {}^{l}/_{\varepsilon} \le {}^{l}/_{\varepsilon_1} \tag{16}$$

Eq. (16) is basically applied to solid columns subjected to centrally-applied static load. In order to extend its application to hollow cross-sections operating under dynamic impact condition and subjected to distributed compressive load, the equation is written in the form (17);

$$\overline{P}_{cr} = \frac{A_*}{\eta}\left[S_y - \left(\frac{S_y}{2\pi}\frac{l}{\varepsilon}\right)^2 \frac{1}{CE_m}\right] \equiv Fp_j;\ {}^{l}/_{\varepsilon} \le {}^{l}/_{\varepsilon_1} \tag{17}$$

For thin-walled sections of $t/b \le 0.08; \eta = 1, A_* \cong 2t(b+h)$. η could reach the ratio S_u/S_y for a very thick walled section [19].

Where; $A_* = A(1-\varphi) \cong 2t(b+h) - 4t^2$ is critical cross-sectional area of hollow column, η is material strain hardening factor, $\overline{P}_{cr}$ is resultant critical load, S_y is yield strength, S_u is ultimate stress, $\varphi = A_i/A$ is void factor, $\varepsilon(=\sqrt{I/A_*})$ is radius of gyration, E_m is elastic modulus, C is end condition factor, $\frac{l}{\varepsilon}$ is slenderness ratio. $A(=bh)$, A_i, h, b *and* t are clearly described in Fig. 5a. It then follows that for thin-walled rectangular cross-sections with external dimension h, b.

$$A_* = \frac{\eta P_{cr}}{S_y\left(1 - aS_y/E_m\right)} \cong 2t(b+h) \tag{18}$$

$a = \frac{\zeta}{4\pi^2}$; and $\zeta = \left(\frac{l}{\varepsilon}\right)^2 C^{-1}$ are constants which depend on Poisson ratio and end condition of the column. This implies that for a structural region identified with uniform cross-section, the critical material thickness t_* is given by;

$${t_*}^2 + \alpha t_* + \beta = 0 \tag{19}$$

Where;

$$\alpha = -(b+h)/2, \beta = \frac{\eta P_{cr}}{4S_y\left(1 - aS_y/E_m\right)} = \frac{1}{4}A_* \tag{20}$$

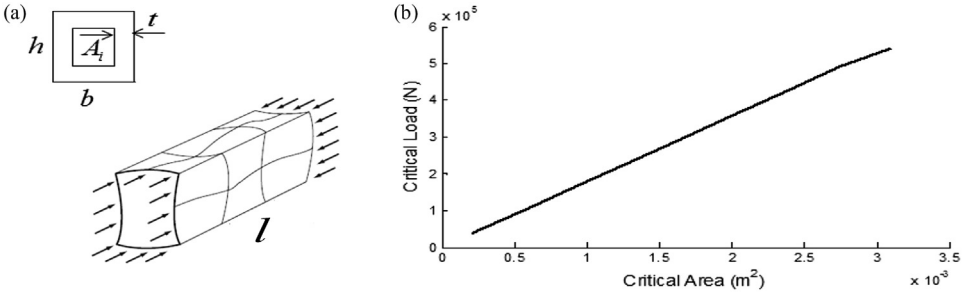

Fig. 5. (a) Locally buckled rectangular box-column and (b) linear dependence of the critical on cross-sectional area.

http://dx.doi.org/10.1016/j.heliyon.2016.e00107

Considering the Euler's column formula (21),

$$P_{cr} = \frac{C\pi^2 E_m I}{l^2} = \frac{C\pi^2 A E_m}{(l/\varepsilon)^2} \tag{21}$$

Where; $E_m I = flexural\, rigidity$

The limiting value $^{l}/_{\varepsilon_1}$ of slenderness ratio is obtained by setting $P_{cr}/A = S_y/2$ such that

$$l/\varepsilon_1 = \left(2\pi^2 C E_m / S_y\right)^{1/2} \tag{22}$$

An intermediate column is verified for a structural member if

$$l/\varepsilon \leq l/\varepsilon_1 \tag{23}$$

2.6. Critical load matching/system adjustment

To ensure that the various structural regions are sufficiently adjusted to the appropriate value of γ and the desired value of absorbable energy ratio r whose performances are already known based on preliminary investigation via LMS method, the guidelines established in (17), (18) and (23) must be followed judiciously. The region with the least P_{cr} indicates the weakest structural member. Since localized failure is anticipated, permanent deformation progresses from the zones of smaller P_{cr} to those of higher P_{cr}. Literally, the critical load of a component reflects the peak force $F_{p,j}$ of the LMS theory. To all intents and purposes, the mean dynamic force which sustains plastic flow could be expressed in terms of the peak force such that both γ and r become universal design variables which are matched between the alternative models by comparing the mean critical load ratio $(\overline{P_{cr2}}/\overline{P_{cr1}})$ of the FE regions to their relative peak force $\left(\overline{F}_{p,2}/\overline{F}_{p,1}\right)$ of the LMS model. This leads to the critical load matching criteria (24) proposed for homogeneous integral body vehicle structure.

$$\overline{P_{cr2}}/\overline{P_{cr1}}\left(\cong \overline{A_{*2}}/\overline{A_{*1}}\right) = \overline{F}_{p,2}/\overline{F}_{p,1} \tag{24}$$

The new decision variable $\overline{A_{*2}}/\overline{A_{*1}}$ was considered in the context of the assumed integral structure with rectangular cross-sections as approximately equal to the ratio of the mean thickness ratio $\overline{t_{*2}}/\overline{t_{*1}}$. This allows for quick formulation of the components. The concept of critical load matching ultimately enhances necessary matching of design variables in the alternative computation models required for making informed decisions in the proposed absorbable energy monitoring scheme. The linear dependence of critical load on cross-sectional area is illustrated in Fig. 5b for an elasto-plastic rectangular column with the following properties; $l/\varepsilon = 530.3384$; $C = 1$; $S_y = 180MPa$; $E = 210GPa$

http://dx.doi.org/10.1016/j.heliyon.2016.e00107

3. Results and discussion

The scope of this work covers preliminary investigation of crash performance of vehicle front-structure using the proposed absorbable energy monitoring scheme and validation of the absorbable energy monitoring system for detailed numerical evaluation of vehicle front structure in crash energy management.

3.1. Preliminary investigation of crash performance of vehicle front Structure using absorbable energy monitoring scheme

This aspect of the study addressed the most fundamental issues that are usually encountered in preliminary vehicle crashworthiness design such as; components formulation for high energy absorption, crash response prediction at various parameter settings and collision conditions, evaluation of desirable crash mode, etc. The 2DOF lumped-mass-spring vehicle impact simulation model was applied for the study.

3.1.1. Pre-planning for high energy absorption

To ensure that the vehicle structure was sufficiently adjusted for high energy absorption in the preliminary design stage, an initial survey of how the system as idealized (in Fig. 1a) may dissipate the total impact energy was conducted. As a good starting point, the spring system was first considered at a balance strength configuration where the absorbable energy ratio (r) was ideally set to unity for initial assessment of the energy absorption performance of the system. The necessary adjustments were then accomplished by studying the histories of energy absorption as the adjustment parameter γ was varied within a suitable range. For the purpose at hand, a good judgment was attained after observing the system performance at selected values of γ in the range $0.6 \leq \gamma \leq 1.6$. The test was conducted at a typical test velocity $(V_0 = 10m/s)$ using a typical engine – to – payload mass ratio (ρ) of 0.25. The results of the energy absorption study presented in Fig. 6 show that adjusting the system towards $\gamma < 1$ did not guarantee

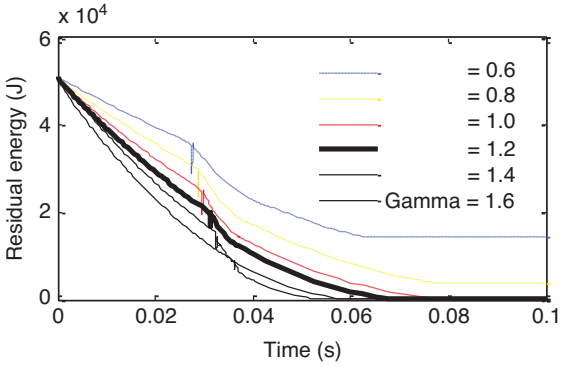

Fig. 6. Residual energy histories at various level of system adjustment.

http://dx.doi.org/10.1016/j.heliyon.2016.e00107

total loss of the initial kinetic energy of the masses within typical test duration of 0.1s. Testing the system with high values of $\gamma \gg 1$ ensured complete loss of the initial kinetic energy but resulted in progressive reduction in the total period of energy absorption due to increasing structural rigidity. The latter trend certainly becomes undesirable at some points since it supports increasing velocity gradient (or high acceleration spikes) of the vehicle masses. The best performance of the system was achieved with the value of adjustment parameter fixed in the range$(1 < \gamma < 1.2)$. At this point choosing a sufficiently constrained upper limit grants the best tolerance in practice.

From the energy absorption study it could be inferred that any configuration of the system leading to a very lower value of $\gamma \ll 1$ may pose unpredictable fatality resulting from high structural flexibility, insufficient energy absorption or high energy transmission while very high value of $\gamma \gg 1.2$ certainly leads to decreasing duration of impact events, high acceleration spikes, poor energy absorption and increasing fatality caused by high structural rigidity. Monitoring the system performances at these abstract parameter ranges (at which prediction of the final condition of the system is extremely difficult) may not provide substantial information required for achieving the key design objectives of the present study.

To formalize the system adjustment rule already introduced for the current problem, the system response (in terms of the displacement, velocity, acceleration of the masses) and deformation of the structural components at; normal (unadjusted) mode where $\gamma = 1$ and sufficiently adjusted mode where $\gamma = 1.2$ were evaluated. The results are presented in Fig. 7a, Fig. 8a, Fig. 9a and Fig. 10a for all investigations at normal mode and Fig. 7b, Fig. 8b, Fig. 9b and Fig.10b for the equivalent adjusted system. The effects of tuning the relative strength of the nonlinear spring (used to model the vehicle structure) in the range $0.3 < r < 3$ were computed and the best performance of the system highlighted at every step of the investigation. The results primarily confirm two possible crash modes $(CM1, CM2)$ of the system; one of which $(CM1)$ is associated with the lower values of $r < 1.9$ while the other prevails in the range of $r \geq 1.9$. The

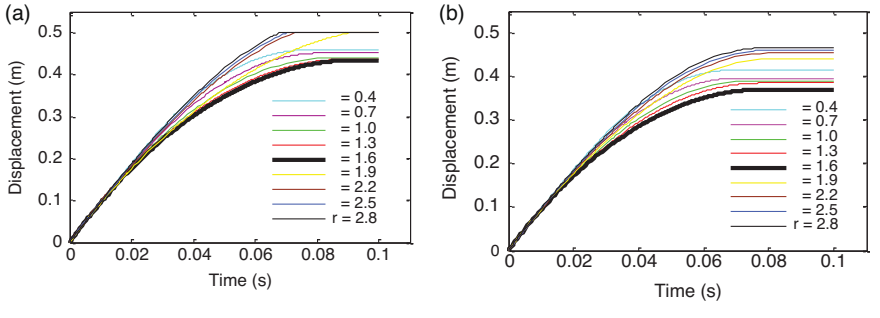

Fig. 7. Displacement histories of the payload mass.

http://dx.doi.org/10.1016/j.heliyon.2016.e00107

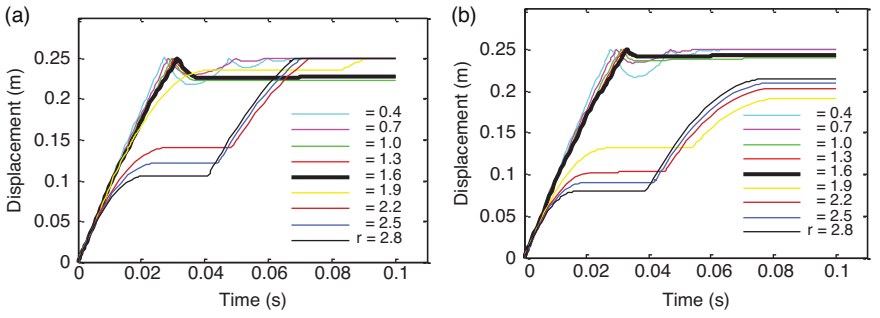

Fig. 8. Displacement histories of the engine mass.

separation of crash modes towards $r = 1.9$ seems to be a major influence on the system response and its effects were monitored throughout the study.

3.1.2. Displacement response of the engine and payload masses

The displacement responses of the engine and the payload masses were calculated on displacement-time plane for the two optional structural adjustment plans. The results recorded for the payload mass (m_1) presented in Fig. 7a are typical of unadjusted system. A relatively high peak displacement of 0.43 m was recorded by m_1 at the best performance of the system. The proposed system adjustment plan of $\gamma = 1.2$ caused a significant reduction of this figure to 0.37 m as illustrated in Fig. 7b. On the other hand, the displacement response of the engine mass (m_2) presented in Fig. 8 provides a greater insight into the effects of the proposed system adjustment rule. The most important outcome recorded at this stage of the investigation is the noticeable rebound of engine mass in the middle of the impact duration after full crushing of the front structure k_2. The engine mass is intuitively expected to experience a significant local rebound for every impact with sufficient energy to guarantee total consumption of k_2. Moreover, it was noticed that the engine rebounds were sustained at varying degrees determined by the relative energy absorption strength of the springs (r). In $CM1$ the engine mass maintained its new position after rebound for the rest of the impact duration when $r \geq 1$ due to

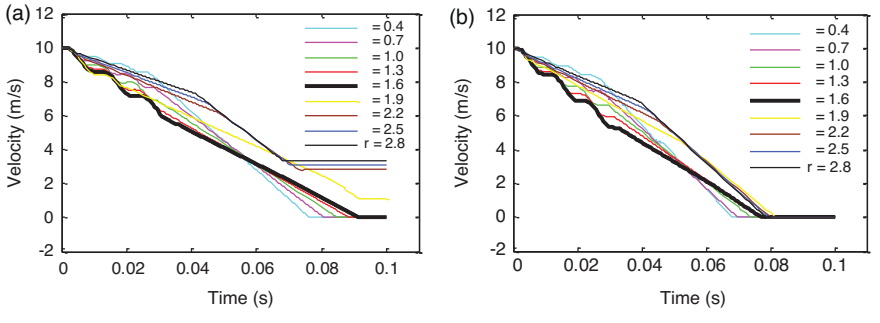

Fig. 9. Velocity responses of the payload mass at; (a) $\gamma = 1$ and (b) $\gamma = 1.2$.

http://dx.doi.org/10.1016/j.heliyon.2016.e00107

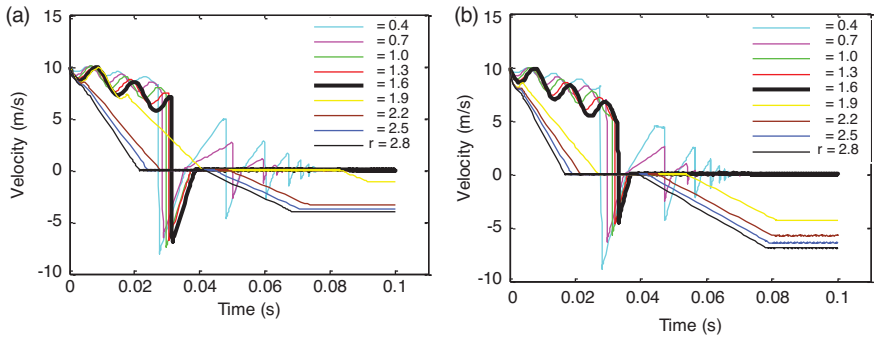

Fig. 10. Velocity responses of the engine mass at; (a) $\gamma = 1$ and (b) $\gamma = 1.2$.

depreciating strength of the interior structure k_1 while for $r < 1$, k_2 was compelled to remain in fully compressed state up to the end of the impact showing increasing tendency for m_2 to experience repeated rebounds as r decreased further. This reflects a severe condition caused by inability of k_2 to absorb a substantial part of the impact energy during deformation suggesting excessive structural compliance. Testing the system at much higher values of $r > 1.9$ which fall within $CM2$ resulted in more severe conditions and complicated behavior where m_2 experienced momentary rest after a considerably high elastic deflection of k_2, while m_1 undergoes full active displacement causing maximum deformation of k_1.

The need to monitor the displacements of vehicle masses and the effect of possible rebound of the engine mass is basically informed by the desire to minimize the deformation of the interior structure in view of the risk of structural intrusion which the reversed motion of the engine mass is capable of increasing. In this regard, the proposed system adjustment resulted in significant improvement of the system which manifested in form of the reduced peak displacement of the payload mass and the minimized rebound of the engine mass highlighted at the system's best performance in Fig. 7b and Fig. 8b respectively.

3.1.3. Velocity response of the engine and payload masses

The velocity responses gathered for the two displaced masses m_1 and m_2 at the specified impact conditions are presented in Fig. 9 and Fig. 10 respectively. The results show that total loss of the initial kinetic energy of the masses within the impact duration is guaranteed for all operations of the system within $CM1$, suggesting what could be desirable in vehicle crashworthiness consideration. Higher values of r falling within $CM2$ resulted in certain levels of unaccounted energy transmission which were however resolved via the proposed system adjustment. Another important observation is the stretching of the impact period over a fairly-smooth sloping velocity path at $r = 1.6$ which grants the lowest

http://dx.doi.org/10.1016/j.heliyon.2016.e00107

possible and most desirable velocity gradient (or acceleration) of the payload mass while operating within $CM1$.

By and large, the velocity histories of the engine mass m_2 recorded at various values of r are presented in Fig. 10. The results show unreasonably high velocity gradient in the effective impact period. The velocity paths reveal periodic restitution of the engine mass with progressively vanishing oscillation peak after the first 20 milliseconds of the impact. The general trend suggests high peak acceleration/deceleration of the engine mass. The main effect of the proposed system adjustment in this regard is further reduction of the effective impact duration and possible rise in acceleration spikes of the masses.

3.1.4. Axial Crush

The deformation response of the impact system was recorded in terms of axial crush of the structural components k_1 and k_2 for every absorbable energy ratio r as shown in Fig. 11 and Fig. 12 respectively. The results gathered in the range of $r < 1.9$ consistently reflect a desirable crash mode of the vehicle structure. The foremost structure k_2 witnessed early and rapid crush while the interior structure k_1 displayed elastic deflection within the first 30 milliseconds of the impact. Thereafter, k_2 got consumed in the 40th millisecond and wedged against the barrier for the rest of the impact duration while, k_1 became fully compliant after 30 milliseconds of the impact and continued to deform at a different rate up to the 70th millisecond when it apparently lost its resistance and then maintained idle motion for the rest of the impact duration. The opposite trends (which of course are undesirable) were recorded with higher values of $r \geq 1.9$. Crash mode change is intuitively expected to occur at a balanced strength condition where $r = 1$. This however is rarely the case in practice since the system may be compelled to maintain initial crash sequence well beyond the balance strength position by inertia forces.

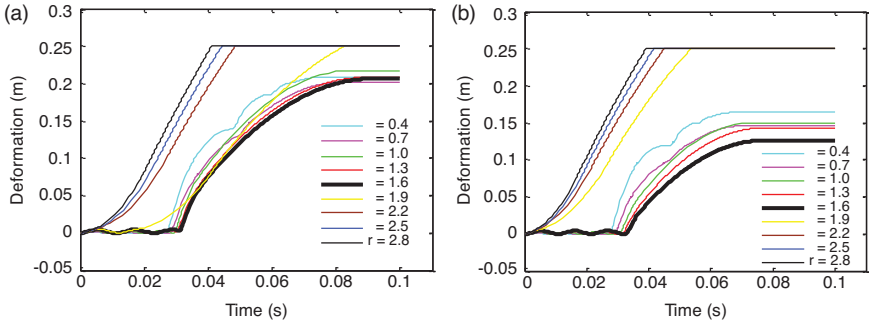

Fig. 11. Calculated axial crush of k_1 at; (a) $\gamma = 1$ and (b) $\gamma = 1.2$.

http://dx.doi.org/10.1016/j.heliyon.2016.e00107

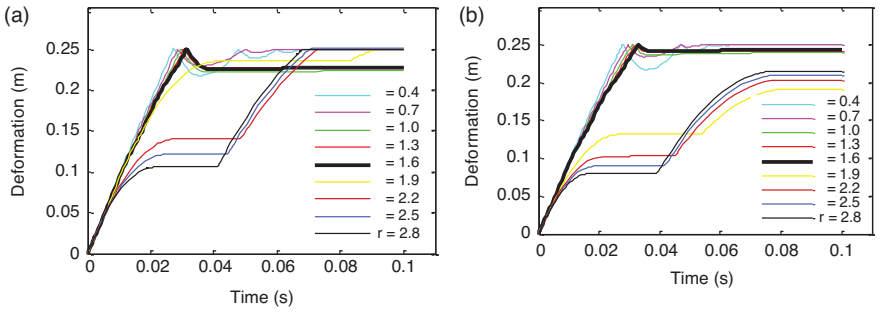

Fig. 12. Calculated axial crush of k_2 at; (a) $\gamma = 1$ and (b) $\gamma = 1.2$.

Observing the deformation histories of the foremost structure k_2 at its normal mode presented in Fig. 12a to a greater detail, it could be inferred that k_2 experienced significant plastic extension after being compressed to its maximum crushable length in the middle of the impact period. Except for $r = 1.6$, the extension of the foremost structure identified in the lower r range as expected was not sustained since the residual compressive force driven by the inertia of the payload mass and the resistance of the interior structure readily compelled the engine mass to undergo repeated rebounds between the fixed barrier and the payload mass leading to multiple extension and compression of k_2. The extension and compression of the foremost structure at a sufficiently high absorbable energy ratio falling within $CM1$ invariably leads to high absorption of impact energy and minimized deformation of the interior structure which are basically desired in crashworthiness design. Moreover, considering the requirements for minimized intrusion of structures into the passenger compartment, a strictly unwanted result is the observed large deformation of k_1 at all values of r while operating the system at normal mode. The proposed system adjustment plan of $\gamma = 1.2$ guaranteed a significant reduction of the peak deformation of the interior structure with the most desirable outcome observed at $r = 1.6$ as shown in Fig. 11b emphasizing the virtue of structural adjustment. Based on what is known so far, an elegant way to achieve this design objective in practice without necessarily increasing the total crushable length of k_1 or altering the already established desirable crash trend is to increase uniformly the stiffness of the structural components a little more within a compliant zone preferably through proper material selection/sizing.

3.1.5. Maximum acceleration/deceleration of the payload mass

It was found that with low r values $\ll 1.9$ the associated high stiffness of the interior structure k_1 supports high peak deceleration of the payload mass observed at a considerably early period of the impact when k_1 is still in the linear range while k_2 has assumed steady force state. The peak deceleration of the payload mass however reduced significantly to an acceptable range as r increased

http://dx.doi.org/10.1016/j.heliyon.2016.e00107

towards 1.6. At high values of $r \geq 1.9$, k_1 became much more compliant leading to a crash mode change, and a further decline in peak deceleration of the payload mass was observed at a later period of the impact when both springs assumed steady force state. Although, further reduction in peak deceleration of the payload mass observed as r value stepped a little further towards 3 is basically desirable in consideration for occupants safety, yet the need to maintain a desirable crash mode which rather lies substantially in the low range of $r < 1.9$ suggests that certain level of trade-off must be implemented in this regard. In line with the popular US Federal Motor Vehicle Safety Standards, an upper limit of acceleration/deceleration of about 30 g is acceptable for the payload mass [7, 11, 20, 21]. Fig. 13 presents the details of the results for the two optional structural adjustment plan.

3.1.6. Effect of engine – to – payload mass ratio (ρ) on the observable crash mode

The study on the effect of engine – to – payload mass ratio (ρ) was conducted for the adjusted system set at the nominal optimal r value of 1.6, considering a moderate impact velocity of 10 m/s and a fixed payload mass of 820 kg. The deformation response of the system was evaluated while the engine – to – payload mass ratio was varied in the range $0.05 \leq \rho \leq 0.5$. The variation of the engine mass produced some significant effects on the crash response of the vehicle structure as presented in Fig. 14(a) and Fig. 14(b). The most important discovery at this level of the study is the non-uniform effects of ρ identified within the sampled space which led to complete deviation from the original desirable crash mode at $\rho = 0.05$ and $\rho = 0.15$. Increasing the engine mass at the studied system configuration ultimately led to reduced peak deformation of the interior structure as highlighted in Fig. 14(a). This result suggests another route to desirable response. However, it is known that increasing the engine mass has

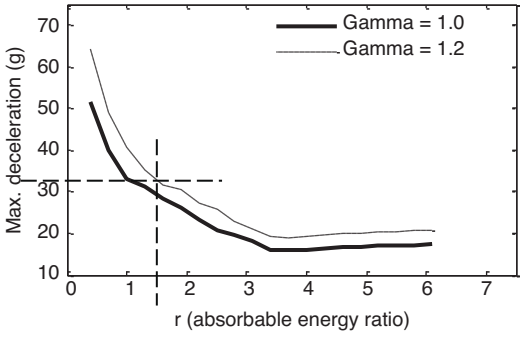

Fig. 13. Maximum decelerations of the payload mass obtained for the various values of absorbable energy ratio.

http://dx.doi.org/10.1016/j.heliyon.2016.e00107

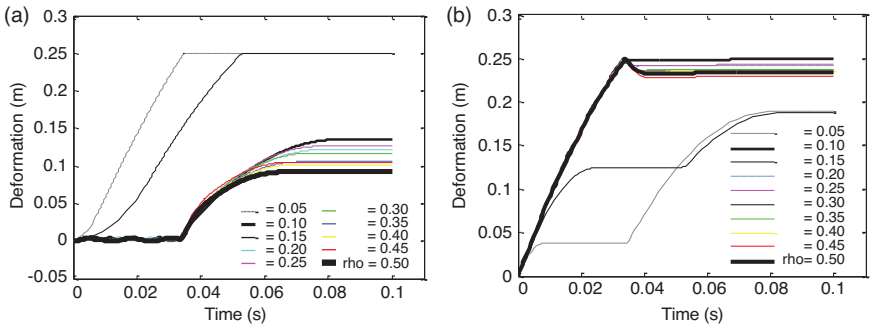

Fig. 14. Effects of engine – to – payload mass ratio on deformation histories of (a) the interior structure k_1 and (b) the foremost structure k_2.

some other undesirable effects in drive energy management, material cost and environmental protection.

3.1.7. Effect of impact velocity (V_0)

Another major issue facing a designer at the early design stage is the unknown effect of the impact velocity V_0 on the observable crash mode. Thus the preliminary investigation is tailored to further examine the system performance at some practical range of V_0 on the observable crash mode of the vehicle structure. The study was conducted for the adjusted system at nominal optimal r with both ρ and m_1 fixed this time at 0.25 and 820 kg respectively. The deformation response of the system was evaluated while $V_0\,(m/s)$ was varied within the range $0 \le V_0 \le 16\,m/s$. The most significant effect of choosing V_0 from the practical range of 0–16 m/s is the changing rate of deformation of the components presented in Fig. 15(a) and Fig. 15(b) for the interior and the foremost structure respectively. The recorded marginal effects tend to diminish towards high impact velocity.

At low enough impact velocity ≤ 3 *m/s,* the interior structure k_1 did not undergo plastic deformation. The elastic deflections recorded by k_1 in this range of impact

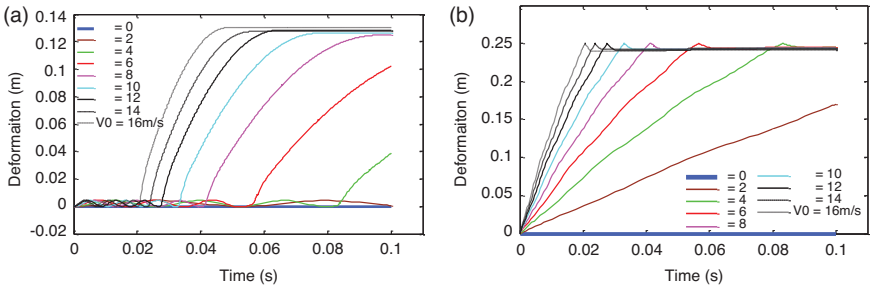

Fig. 15. Effects of V_0 on the deformation response of (a) the interior structure k_1 and (b) foremost structurek_2.

http://dx.doi.org/10.1016/j.heliyon.2016.e00107

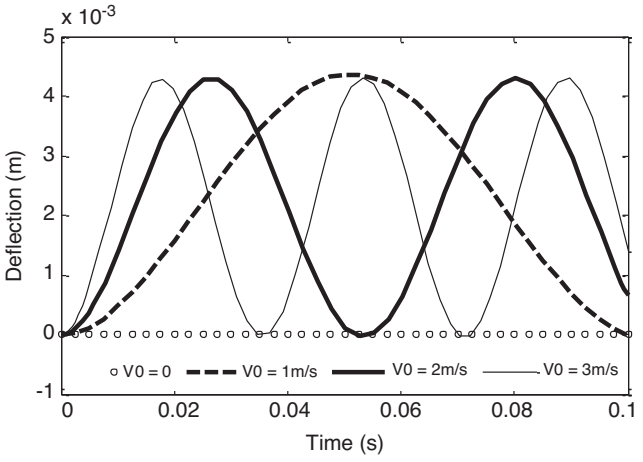

Fig. 16. Time histories of deflections of k_1 at low impact velocities.

velocity are magnified in Fig. 16. The observable effect of increasing impact velocity within the elastic range was that of increasing the frequency of vibration of the interior structure, while the amplitude of vibration remains apparently uniform.

Further investigation on the effects of impact velocity on the condition for crash mode change was conducted. It was also observed that V_0 has no significant effect on the condition for crash mode change. The detail of this result is not presented in this paper.

The results of the preliminary study (achieved through LMS system) suggest that the best performance of the system could be achieved with the value of r selected from the range $1.6 \leq r < 1.9$. The results obtained at $r = 1.6$ (which corresponds to greater energy absorption of 61.5% of the total absorbable energy through the deformation of the foremost structure) were therefore highlighted all through as the nominal best performance of the system while the bounded space $(1.6 \leq r < 1.9)$ is considered a prospective domain for a more detailed crashworthiness optimization study.

3.1.8. Design of components

The preliminary survey of the vehicle impact problem presented above was conducted for a homogenous unit body vehicle structure assuming the engine mass to be centrally mounted along the front frame i.e. $L_{C,2}/L_{C,1} = 1$. The results led to the following deductions;

i. Monitoring the system response at various absorbable energy ratios is capable of revealing certain desirable stiffness and damping properties that could lead to desirable response in vehicle crashworthiness design

http://dx.doi.org/10.1016/j.heliyon.2016.e00107

ii. Although observations of the system at comparable structural strength ratios but different γ values led to overall similarity in the general crash trend yet significant difference in crash performance indices could be observed with such system adjustments

iii. Desirable crash response is guaranteed with high energy absorption (up to 60%) through deformation of the foremost structure.

This information provides the background knowledge required to make appropriate decision during component formulation. The formulation of the components requires that, the dynamic stiffnesses which guarantee various energy absorption patterns are first evaluated for the system using the LMS procedure. The choices are then guided by the need to meet desired energy absorption plan, correct deformation sequence and optimum acceleration of the occupant (or payload mass). In the study, components stiffnesses were analyzed over a wide range of r and the results are presented in Fig. 17. The most desirable system performance was recorded at $r = 1.6$. By and large, $r = 1.6$ lies in the vicinity of crash mode change and corresponds to a rather poor structural configuration where k_1 is considerably weaker.

In line with real vehicle structural requirement, the result is not acceptable as it is. The interior structure due to their location in the system is usually designed to support a greater (static and dynamic) service loads. This implies that they are rather made stronger. To achieve this important attribute in practice (while retaining the already established condition for improved crash performance) requires that the system is further adjusted such that $L_{C,2}/L_{C,1} \gg 1$. This consideration does not only ensure that less contribution to the total energy absorption is achieved with a stronger interior structure, but also allays the fear of undesirable crash mode within the entire vehicle front structure since desirable

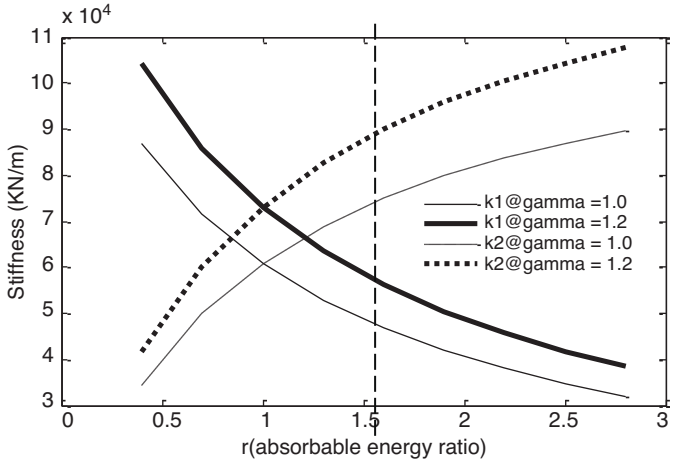

Fig. 17. Stiffness of structural components at various absorbable energy ratios.

http://dx.doi.org/10.1016/j.heliyon.2016.e00107

energy absorption pattern are achieved at a value of r that lies intimately in the desirable CM range.

3.1.9. Validation of the proposed 2DOF LMS model for parametric structural crashworthiness design optimization using vehicle-to-pole impact experiment

To allay the fear of reaching invalid conclusion in the present study, the performance of the proposed 2DOF LMS model in predicting real vehicle crash response was evaluated using experimental central pole-impact test data reported in [22]. The central pole-impact test was conducted for a standard Ford Crown Fiesta at a moderate impact speed of 35 km/h. From the report, wide-band data representing the raw longitudinal acceleration/deceleration of the body mass $(\ddot{x}_1)$ recorded by an accelerometer attached close to the center of gravity of the vehicle during the test period was first filtered with a Butter-worth 3rd-oder low-pass digital filter to obtain a clear representation of the result. The integral $\int(\ddot{x}_1)dt$ and the double integral $\iint(\ddot{x}_1)dt$ of the acceleration response were then evaluated numerically to obtain the velocity response $\dot{x}_1$ and the displacement response x_1 of the body mass m_1 respectively. The collection of the results as reported in [9, 16] is presented in Fig. 18(a).

The parameters of the 2DOF LMS model were then set to give adequate prediction of the vehicle crash response at similar configuration of the system. Since the solution of the impact system via the LMS method depends on crush behavior (i.e. force-deformation characteristics) of the components which are not known for the existing Ford Crown Fiesta, assigning values for the crush parameters p_j, q_j, s_j, $d_{s,j}$ and $L_{C,j}$ may involve certain level of trial and error. The typical values of the crush parameters (see Table 1) which are already known from the preliminary study, and from existing reports [7, 11], were first selected for the 2DOF virtual

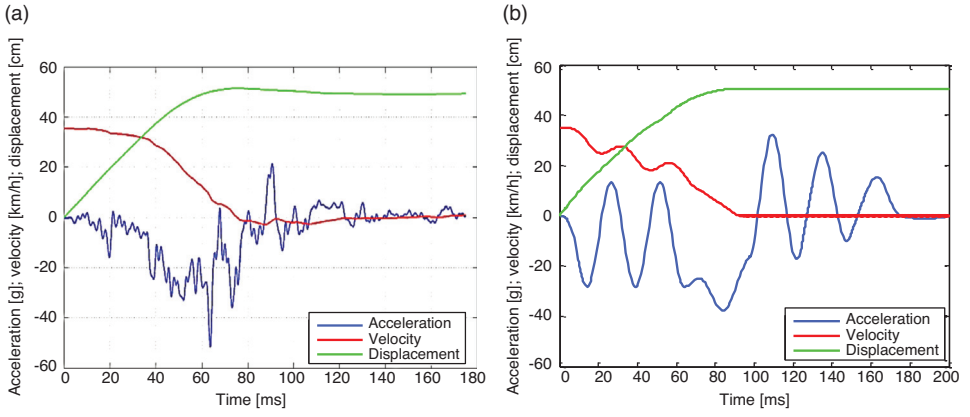

Fig. 18. (a) the actual test data [22] and (b) the predicted crash response of the experimental pole-impact test via the proposed 2DOF LMS model.

http://dx.doi.org/10.1016/j.heliyon.2016.e00107

test. The predicted results agree reasonably with the actual test data as shown in Fig. 18(b). The effects of using other possible set of values for the crush parameters such as; $p_j = 0.25$, $q_j 0.35$, $s_j = 3$ and $p_j = 0.35$, $q_j = 0.45$, $s_j = 3$ which also ensure convergence of the response are presented in Fig. 19(a) and Fig. 19(b) respectively for comparison. Other values of p_j, q_j, s_j, $d_{s,j}$ and $L_{C,j}$ tried outside the range presented did not guarantee adequate convergence of the predicted result to the experimental data. The results presented in Fig. 19 (a) represents the best performance of the predictive model. From the detail of the results gathered so far from the validation test, the range of values of p_j, q_j, s_j, $d_{s,j}$ and $L_{C,j}$ that guarantee convergence of the solution is sufficiently close, hence assuming average (constant) value for each of the parameters in a preliminary optimization study such as the one conducted in section 3.1 above remains valid.

3.2. Validation of the proposed absorbable energy monitoring scheme using FE model

To validate the proposed absorbable energy monitoring scheme proposed for preliminary crashworthiness design a typical example of the vehicle impact problem was constructed using FE modeling procedure. The crumple zones designated $L_{C,1}$ and $L_{C,2}$ were first specified to conform to real vehicle structural requirements and the procedure described in section 2.5 was followed strictly to arrive at the critical loads of the components. The equivalent LMS model was then formulated (assuming the same component crush characteristics with the FE model as given in Table 4) and applied for initial assessment of the system performance over a wide parameter range following similar procedure as the one already discussed in section 3.1. Based on the results of the LMS-system-based preliminary investigation and the critical load matching criteria (24), the geometry

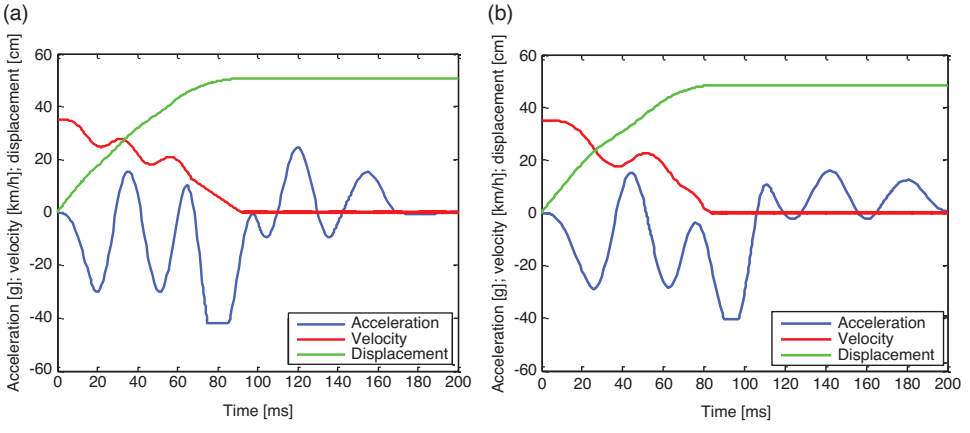

Fig. 19. The predicted crash response of the experimental pole-impact test via the proposed 2DOF LMS model using (a) $p_j = 0.25$, $q_j 0.35$ and (b) $p_j = 0.35$, $q_j = 0.45$, $s_j = 3$.

http://dx.doi.org/10.1016/j.heliyon.2016.e00107

Table 4. Data for the LMS model applied in the validation study.

Symbol	V_0	m_1	ρ	$L_{c,1}$	$L_{c,2}$	p_1	p_2	q_1	q_2	s_1	s_2	γ	r
Value	10	820	0.25	0.35	0.75	0.01	0.02	0.015	0.025	3	3	1.2	1.6
Unit	m/s	kg		m	m								

$\overline{F}_{p,1} = 217.88(kN)$; $\overline{F}_{p,2} = 161.88(kN)$; $\overline{F}_{s,1} = 72.62(kN)$; $\overline{F}_{s,2} = 56.92(kN)$; $\overline{k}_1 = 62.251(MN/m)$; $\overline{k}_2 = 10.792(MN/m)$; $\overline{F}_{p,2}/\overline{F}_{p,1} = 0.743$.

and the mechanical properties of the components were then adjusted in the FE simulation model to conform to the desirable energy absorption plan of $r = 1.6$ as given in Table 5. All other necessary considerations to ensure good performance of the system were observed. At a comparable structural configuration, the crash behaviors of the system predicted by the two models were evaluated and compared. In the exemplified direct frontal impact only the axial displacement of the masses measured in the direction perpendicular to the barrier was used in comparing the resulting crash modes. The axial crush recorded by the foremost structure k_2 and the interior structure k_1 are presented in Fig. 20. Although the predicted crash performance index corresponds substantially between the two models yet the result of the LMS model indicates more delayed plastic deformation of the interior structure and relatively low general instantaneous axial crush which resulted in the extension of the predicted total impact period. Nevertheless, the level of agreement achieved between the results of the models suggests that the unknown solution of the studied vehicle impact system in terms of the desirable energy absorption plan and desirable crash mode could be well predicted by the proposed AEMS. Further comparison in terms of the acceleration/deceleration of the payload mass was not possible since the FE model accounts separately for the structural mass which was rather lumped together with the body mass as the payload mass in line with the

Table 5. Data for the FE model applied in the validation study.

Design variables Sampling space	$b(m)$	$h(m)$	$t(mm)$	$L_{Cj}(m)$	$A_*(m^2) \times 10^{-4}$	$P_{cr}(N) \times 10^5$	$\overline{P_{cr2}}/\overline{P_{cr1}}$
$k_{1'}$	0.09	0.15	1.50	0.35	7.20	1.294	0.739
$k_{1'''}$	0.09	0.15	1.20	0.35	5.76	1.036	
$k_{2'}$	0.09	0.15	1.00	0.75	4.80	0.861	
$k_{2''}$	0.09	0.15	1.00	0.75	4.80	0.861	

Material properties: $S_y = 180\,MPa$; $E = 210\,GPa$; end condition of components $C = 1$; material type – general elastoplastic.

http://dx.doi.org/10.1016/j.heliyon.2016.e00107

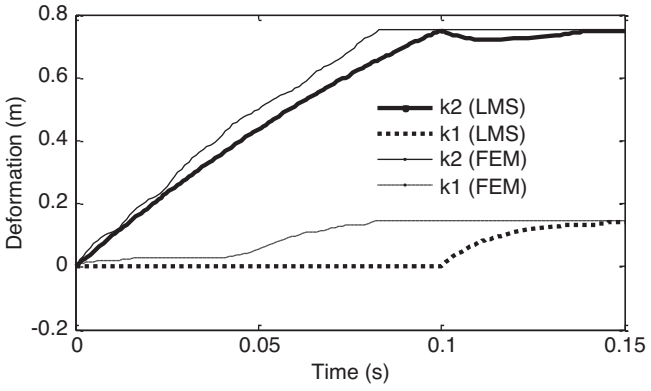

Fig. 20. The comparison of deformation histories of the interior structure k_1 and the foremost structure k_2 predicted by LMS and FEM methods at; $\overline{F}p_2/Fp_1 = 0.743$ and $\overline{P_{cr2}}/\overline{P_{cr1}} = 0.739$ respectively.

standard LMS modeling procedure. However, at the current level of system adjustment, an acceptable peak payload mass deceleration of 23 g was predicted for the system via the LMS system.

The gross motion of the impact system captured at discrete time intervals of 20 milliseconds presented in Fig. 21 show the time history of nodal displacement gathered within 100 milliseconds of the impact duration.

The results of the FE study further confirm that the nominal optimal absorbable energy ratio of $r = 1.6$ is capable of producing a high performance system which guarantees total absorption of the impact energy with desirable crash mode; featuring minimized deformation of the interior structure whose effect is that of ensuring reduced structural intrusion into the passenger compartment. Since the crash behavior of the full vehicle model is substantially predicted at the present

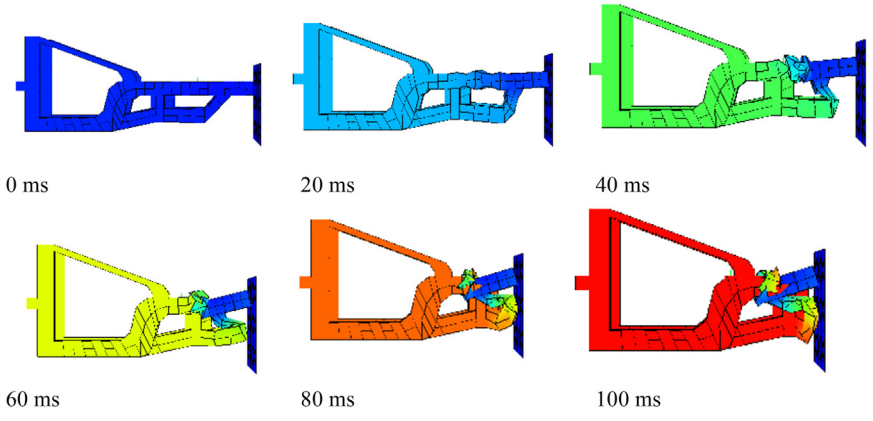

Fig. 21. Gross motion of the vehicle front structure captured at 20 milliseconds intervals of the impact duration.

http://dx.doi.org/10.1016/j.heliyon.2016.e00107

level of structural details, the success of any further optimization at full development of the prototype is guaranteed.

However, it is noted that prediction of crash behavior of vehicle front structure in frontal impacts based on critical load capacities of the members averaged for two distinct structural regions may not guarantee all the needed accuracy for a detailed optimization study (involving full vehicle model). Such cases require more detailed identification of structural regions with significantly non-uniform cross–sections and material make-up. An appropriate method in such instances would therefore account for the wider variation in component geometry and material properties. This fact highlights the limitation of the proposed AEMS in its current form. Future works along this line would be directed towards improving the application of the AEMS beyond this limitation by developing a more robust framework for predicting the distribution of impact load within the various structural regions.

4. Conclusion

This paper presents a new design concept called absorbable energy monitoring scheme (AEMS), proposed for preliminary design for vehicle structural crashworthiness. The application of AEMS in a typical vehicle crashworthiness design is demonstrated. The two basic computation methods including; the LMS system and the FEM were applied successfully for analyzing the impact system. New procedures for calculating the dynamic resistance and the critical load/failure condition of the components under distributed impact load were developed. This allowed for matching of design variables between the alternative computation models and successful application of the two computation methods for the necessary preliminary design investigations. Although this approach to the design problem may be seen as further complication of the existing design procedures capable of causing initial delay of the solution process, yet the effort is fully rewarded by the resulting stability of the computation process and overall savings in computation time that collectively enhanced extensive investigation of the crash behaviors of the studied impact problem beyond the limitations of the alternative computation methods. In the context of absorbable energy monitoring scheme, the mutual agreement achieved in terms of the predicted crash mode and the energy absorption indices of the system between the two computational models suggests the adequacy of the proposed critical load matching criteria for preliminary crash performance evaluation of vehicle structure. For the particular system studied, the overall results further suggest that ensuring sufficiently high (>60%) contribution to energy absorption through deformation of the foremost structures guarantees good crash performance of the vehicle front structures. With this condition well attained for a typical design problem the selection of viable parameter range capable of revealing the most desirable system response in a stretch of optimization study becomes much more straightforward and reliable.

http://dx.doi.org/10.1016/j.heliyon.2016.e00107

Declarations

Author contribution statement

Sunday M. Ofochebe: Conceived and designed the experiments; Analyzed and interpreted the data; Wrote the paper.

Samuel O. Enibe: Contributed reagents, materials, analysis tools or data.

Chigbogu G. Ozoegwu: Analyzed and interpreted the data.

Funding statement

This research did not receive any specific grant from funding agencies in the public, commercial, or not-for-profit sectors.

Competing interest statement

The authors declare no conflict of interest.

Additional information

No additional information is available for this paper.

References

[1] Z.Q. Cheng, J.G. Thacker, W.D. Pilkey, W.T. Hollowell, S.W. Reagan, E.M. Sieveka, Experiences in reverse-engineering of a finite element automobile crash model, Finite Elem. Anal. Des. 37 (2001) 843–860.

[2] K. Hamza, K. Saitou, Design for Structural Crashworthiness Using Equivalent Mechanism Approximations, J. Mech. Des. 127 (2005) 485–492.

[3] H.-P. Wang, C.-T. Wu, Y. Guo, M.E. Botkin, A coupled meshfree/finite element method for automotive crashworthiness simulations, Int. J. Impact Eng. 36 (2009) 1210–1222.

[4] S. Newstead, M. Cameron, C.M. Le, Vehicle crashworthiness ratings and crashworthiness by year of vehicle manufacture: Victoria and NSW crashes during 1987-97, Queensland crashes during 1991-96, Monash University of Accident Research Centre, Wellington Road, Clayton Victoria, 1999.

[5] M.M. Kamal, Analysis and Simulation of Vehicle to Barrier Impact, International Automobile Safety Conference, Detroit Michigan, 1970.

[6] C.C. Alexandra, G.M. Stuart, R.R. Samaha, Lumped parameter modeling of frontal offset impacts, SAE paper (1995) 950651.

 http://dx.doi.org/10.1016/j.heliyon.2016.e00107

[7] A.I. King, B.B. Fileta, C.C. Chou, H.F. Mahmood, H.J. Mertz, J. Wismans, P. D. Bois, T.B. Khalil, Vehicle crashworthiness and occupant protection, American Iron and Steel Institute 2000 Town Center, Southfield, Michigan, 48075, 2004.

[8] K. Hamza, K. Saitou, Crashworthiness design using meta-models for approximating the response of structural members, MDP-8 Cairo University Conference Proceeding of MDP-8, Cairo University Conference on Mechanical Design and Production, Cairo, Egypt, 2004 January 4-6.

[9] W. Pawlus, K.G. Robbersmyr, H.R. Karimi, Mathematical modeling and parameters estimation of a car crash using data-based regressive model approach, Appl. Math. Model. 35 (2011) 5091–5107.

[10] J. Marzbanrad, M. Pahlavani, Parameter determination of a vehicle 5-DOF Model to simulate Occupant deceleration in a frontal crash, World Acad. Sci. Eng. Technol. (55) (2011) 336.

[11] S.M. Ofochebe, C.G. Ozoegwu, S.O. Enibe, Performance evaluation of vehicle front structure in crash energy management using lumped mass spring system, Advanced Modeling and Simulation in Engineering Sciences 2 (2) (2015).

[12] J.Y. Bruno, F. Hartemann, C. Thomas, A. Fayon, C. Tarriere, Correlation between thoracic lesions and force values measured at the shoulder of 92 belted occupants involved in real accidents, SAE Paper (1978) 780892.

[13] D. Cesari, M. Ramet, Evaluation of human tolerance in frontal impacts, SAE Paper (1979) 791032.

[14] J.Y. Bruno, X. Trosseille, J.Y. Coz, Thoracic injury risk in front car crashes with occupant restrained with belt load limiter, SAE Paper (1998) 983166.

[15] T. Tenga, F. Chang, Y. Liu, C. Peng, Analysis of dynamic response of vehicle occupant in frontal crash using multibody dynamics method, Math. Comput. Model. 48 (2008) 1724–1736.

[16] W. Pawlus, H.R. Karimi, K.G. Robbersmyr, Mathematical modeling of a vehicle crash test based on elasto-plastic unloading scenarios of spring-mass models, Int. J. Adv. Manuf. Technol. 55 (2010) 369–378.

[17] S.W. Kirkpatrick, J.W. Simons, T.H. Antoun, Development and validation of high fidelity vehicle crash simulation models, IJCrash'98 - International Crashworthiness Conference, USA, 1998.

[18] G.B. Richards, J.K. Nisbett, Shigley's Mechanical Engineering Design, Eight Edition, McGraw-Hill Companies Inc, New York, 2008.

 http://dx.doi.org/10.1016/j.heliyon.2016.e00107

[19] H.F. Mahmood, A. Paluszny, Axial Collapse of thin wall cylindrical column, Fifth International Conference on Vehicular Structural Mechanics, SAE Paper, Detroit, 1984 840727.

[20] C.J. Kahane, National Highway Traffic Safety Administration's evaluations of Federal Motor Vehicle Safety Standards, SAE (1984) 840902.

[21] F.V. Curtis, Dynamic modeling of automobile structures from test data, General Motors Research Corporation Report, GM–19, 1979.

[22] K.G. Robbersmyr, Calibration test of a standard ford fiesta 1. 1l, model year 1987, according to NS - EN 12767, Technical Report 43/2004 Agder Research, Grimstad, 2004.

 http://dx.doi.org/10.1016/j.heliyon.2016.e00107